ISSN 1330–0016
CODEN FIZBE7

MEASUREMENT OF THE NEUTRON'S ELECTRIC FORM FACTOR $G_{\mathrm{E}}^{\mathrm{n}}$ VIA DOUBLY POLARIZED, QUASI-ELASTIC SCATTERING AT JEFFERSON LAB

FRANK R. WESSELMANN

University of Virginia, Charlottesville, Virginia 22904, USA
for the E93-026 Collaboration

Received 6 November 2003; Accepted 24 May 2004
Online 22 November 2004

We determined the electric form factor of the neutron $G_{\mathrm{E}}^{\mathrm{n}}$ via the reaction $\vec{\mathrm{d}}(\vec{\mathrm{e}},\mathrm{e}'\mathrm{n})\mathrm{p}$ using a longitudinally polarized electron beam and a frozen, polarized $^{15}\mathrm{ND}_3$ target at Jefferson Lab. The knocked out neutrons were detected in a segmented plastic scintillator in coincidence with the quasi-elastically scattered electrons which were tracked in Hall C's High Momentum Spectrometer. To extract $G_{\mathrm{E}}^{\mathrm{n}}$, we compared the experimental beam–target asymmetry with theoretical calculations based on different $G_{\mathrm{E}}^{\mathrm{n}}$ models. We report the results of the fall 2001 run at $Q^2 = 0.5$ and 1.0 $(\mathrm{GeV}/c)^2$.

PACS numbers: 13.40.Gp, 14.20.Dh UDC 539.12

Keywords: neutron, electric form factor, polarized electron beam, polarized $^{15}\mathrm{ND}_3$ target, neutron - electron coincidences

1. Introduction

Elastic form factors are among the earliest approaches utilized to represent the internal structure of nucleons. They lend themselves to particularly inituitive interpretation by relating them to charge and magnetization distributions, and have allowed for a consistent first-order approximation. However, since the neutron carries no net charge, this approximation of the neutron's electric form factor is simply zero, regardless of kinematics. This makes $G_{\mathrm{E}}^{\mathrm{n}}$ particularly sensitive to the internal structure.

Despite a significant number of measurements, $G_{\mathrm{E}}^{\mathrm{n}}$ is still poorly known. Until recently, existing data covered only a limited kinematic range, up to an interaction energy of $Q^2 \sim 0.5$ $(\mathrm{GeV}/c)^2$, and most of those determinations suffer from significant systematic limitations due to wave function models. Less model dependent cross section methods are limited by the value of $G_{\mathrm{E}}^{\mathrm{n}}$ being dominated by the larger $G_{\mathrm{M}}^{\mathrm{n}}$. New methods have been developed using polarization observables, bypass-

ing these issues. The particular approach employed in the measurement discussed here extracts $G_{\mathrm{E}}^{\mathrm{n}}$ from the cross section asymmetry in scattering of electrons with opposite helicity states off a polarized target.

Introducing polarization as an observable in the scattering process requires an adjustment to the equation relating the cross section and the form factors. For the Sachs version of the form factors, this is the Rosenbluth equation

$$\left(\frac{\mathrm{d}\sigma}{\mathrm{d}\Omega}\right) = \left(\frac{\mathrm{d}\sigma}{\mathrm{d}\Omega}\right)_{\mathrm{Mott}} \times \left[\frac{G_{\mathrm{E}}^2 + \tau G_{\mathrm{M}}^2}{1+\tau} + 2\tau G_{\mathrm{M}}^2 \tan^2\frac{\theta_{\mathrm{e}}}{2}\right]. \tag{1}$$

Here, θ_{e} is the electron scattering angle and $\tau = Q^2/4M^2$ is a purely kinematic factor. To account for polarization ($\mathcal{P}$), a second term (Δ) is added to the unpolarized expression (Σ)

$$\frac{\mathrm{d}\sigma}{\mathrm{d}\Omega} \sim \Sigma + \mathcal{P}\Delta.$$

The asymmetry between the cross sections of opposite helicity states ($\pm\mathcal{P}$) corresponds to the ratio of the polarization-dependent term to the plain unpolarized term

$$A^{\mathrm{V}} = \frac{\sigma_+ - \sigma_-}{\sigma_+ + \sigma_-} = \frac{\Delta}{\Sigma}.$$

We can simplify this expression by imposing additional requirements on the scattering process. If we arrange for the nucleon's polarization vector to lay within the plane defined by the elastically scattered electron and further that it is perpendicular to the q-vector, the beam helicity asymmetry reduces to an interference term between the electric and the magnetic form factor [1]

$$A^{\mathrm{V}} = \frac{-2\sqrt{\tau(1+\tau)}\,\tan\frac{\theta_{\mathrm{e}}}{2}\,G_{\mathrm{E}}\,G_{\mathrm{M}}}{G_{\mathrm{E}}^2 + \tau[1+2(1+\tau)\tan^2\frac{\theta_{\mathrm{e}}}{2}]\,G_{\mathrm{M}}^2}. \tag{2}$$

The lack of a free-neutron target can be addressed by using deuterium (^{2}H) nuclei, consisting of a loosely bound neutron–proton pair. The requirement of elastic scattering then translates into quasi-free quasi-elastic scattering, meaning the struck neutron's momentum differs only trivially from the momentum transfer q.

2. Experimental setup

The experiment was conducted in the fall of 2001 in experimental hall C of the Thomas Jefferson National Accelerator Facility (Jefferson Lab) in Newport News, Virginia, USA. The scattering interaction studied occurred between the longitudinally polarized electron beam and a polarized solid target consisting of cryogenically frozen deuterated ammonia, $^{15}ND_3$. To ensure that our data were based on quasi-elastic scattering off a neutron in the target, the neutron and the scattered electron were detected in coincidence.

Jefferson Lab provides a high current, continuous electron beam with longitudinal polarization as high as 80% [2]. The actual polarization was measured periodically with the standard Hall C double-arm Moller polarimeter [3]. The actual effective beam polarization was $\sim$ 78% for our $Q^2 = 0.5$ $(\mathrm{GeV}/c)^2$ running period but it was less than 72% for the $Q^2 = 1.0$ $(\mathrm{GeV}/c)^2$ data set. The data were taken at respective beam energies of 2.3 GeV and 3.5 GeV with a current of about 100 nA, limited by the solid target.

The target apparatus [4] consists of a pair of superconducting Helmholtz coils inside a vacuum vessel. They can generate a polarizing field of 5 T which the electron beam traverses. The target material is contained in a small cylindrical cup, several of which are attached to a supporting ladder. A thin-walled pipe reaching into the center of the vacuum vessel allows the insertion of the ladder into the field while immersing it in liquid helium. An external mechanism moves the ladder and can thus position one of the material cups inside the field and into the beam. A set of pumps extracts the boiled-off helium, increasing the rate of evaporation and thereby reducing temperature of the liquid helium and the target material to $\sim$ 1 K.

Wave guides attached to the target ladder funnel microwaves toward the target material. These drive a "dynamic nuclear polarization" process [5] which artificially enhances a selected polarization state. The achieved polarization is continually measured via an NMR system [6] utilizing a wire loop pickup coil embedded in the target material. The dynamic nature of the polarization method requires the beam to be evenly distributed across the target volume as the NMR system cannot detect localized variations in the polarization. This was achieved by rastering the beam across the face of the target using two dipole magnets driven with AC currents, creating independent horizontal and vertical deflections. Also, the polarizing field itself deflects the electron beam, resulting in non-normal trajectories inside the target and steering the beam away from the collection dump downstream of the target. By installing a two-dipole chicane just upstream of the target, the pre-scattering deflection was offset and a custom absorber replaced the standard beam dump.

The scattered electrons were detected in Hall C's standard High Momentum Spectrometer. It consists of three acceptance-shaping quadrupoles and a momentum-selecting dipole. A shielded detector hut contained scintillator hodoscopes, wire drift chambers, a gas Cerenkov detector and a lead-glass calorimeter. Together, these detectors provided event timing, particle identification and track slopes and position. Well established reconstruction matrices then allowed the determination of the scattering events' geometry and energy.

For each scattering event seen by the HMS, coincidence nucleons were identified in a custom built neutron calorimeter. This detector consisted of six layers of segmented plastic scintillator material, arranged in horizontal bars transverse to the path of any scattering products. The bulk detector captured and converted protons and neutrons ejected from the target while two thin layers of scintillator material at the front of the detector efficiently distinguished between charged protons and neutral particles. The location and energy signature of the particles' absorption was used to establish coincidence events and nucleon kinematics.

3. *Analysis and results*

In the first stage of the data analysis process, the raw detector data were used to recreate the scattering events by identifying particle tracks and coincidences. The results were stored in Ntuples which, in a second step, were then used to find the number of events for each beam helicity subject to selection cuts and kinematic bins. These counts, together with various systematic values, were then used to calculate a final experimental asymmetry value

$$A_{\mathrm{ed}}^{\mathrm{V}} = \frac{1}{f\,\mathcal{R}_{\mathrm{bkgnd}}} \sum_{\mathrm{runs}} \frac{w_i}{\mathcal{P}_{\mathrm{beam}}^{i}\mathcal{P}_{\mathrm{target}}^{i}} \times \left(\frac{\frac{N^+}{Q^+} - \frac{N^-}{Q^-}}{\frac{N^+}{Q^+} + \frac{N^-}{Q^-}} \right)_i . \tag{3}$$

Each run's event counts for positive and negative beam helicity ($N^{\pm}$) are normalized by the associated beam charge ($Q^{\pm}$) to form a raw event asymmetry. After rescaling these according to beam and target polarizations, the runs are averaged, weighed by statistics (w_i). Finally, an average background correction ($\mathcal{R}_{\mathrm{bkgnd}}$) and target dilution factor (f) are applied to obtain the experimental value for the vector asymmetry $A_{\mathrm{ed}}^{\mathrm{V}}$.

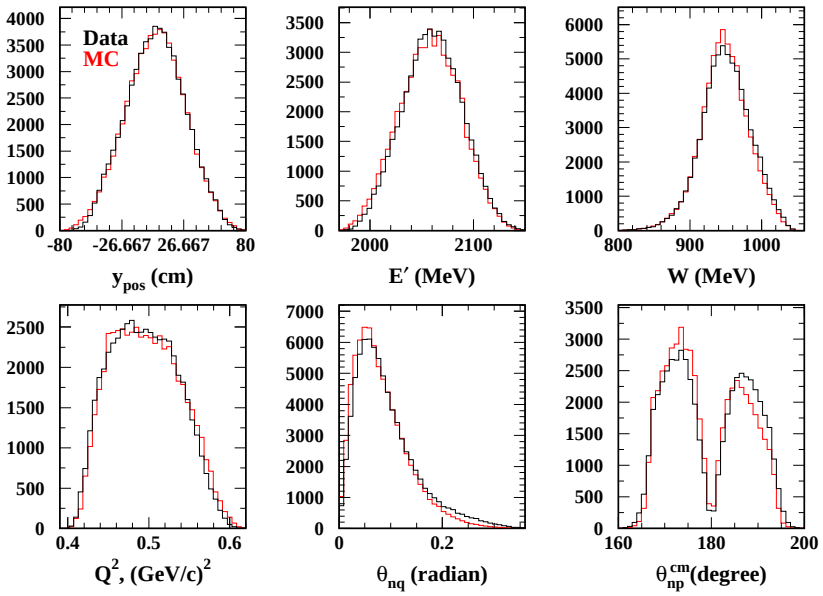

Fig. 1. Comparison of event distribuitions for data and simulation. Sample distributions for some relevant kinematic variables are shown: horizontal neutron track angle (y_{pos}), scattered electron energy (E') and deduced momentum transfer (Q^2) and missing mass (W), as well as the angle between q-vector and neutron momentum in the lab frame (θ_{nq}) and in the center of mass frame (θ_{np}). A single overall normalization factor has been applied.

Maximum correlation between the counts and the associated charge was established by DAQ-gating the beam current signal prior to accumulating the charge. This eliminated any DAQ-related dead time and allowed helicity separation. The background, or accidental, rate was determined by intentionally mis-timing the coincidence requirement. A special analysis effort determined the background rate dependence of the event reconstruction. Similarly, it was established that the background's asymmetry was statistically insignificant.

The dilution factor accounts for scattering events due to interactions with materials other than the desired target, such as container walls or cooling helium. The actual value was determined by comparing the rates from well known test targets with Monte Carlo simulations of the test and actual targets.

The experimentally determined asymmetry is compared to model calculations based on various alternative values of $G_{\mathrm{E}}^{\mathrm{n}}$. Fitting the experiment's result to an interpolation between the various model values determines a corresponding value for $G_{\mathrm{E}}^{\mathrm{n}}$. Since the actual value of the asymmetry is not known independently, the simulation was expected to recreate the otherwise not relevant event rates quite well, as is shown in Fig. 1.

The Monte Carlo simulation was based on the MCEEP package [7]. Its primary purpose was to properly determine $A_{\mathrm{ed}}^{\mathrm{V}}$ for a given $G_{\mathrm{E}}^{\mathrm{n}}$ (based on calculations in Ref. [9]), but it also accounted for radiative corrections and final-state interactions. Nuclear corrections, such as the impact of the extra neutron in ^{15}N were also treated here. A model of the neutron detector and an implementation of the HMS simulation SIMC [8] were included to properly treat acceptance and kinematics.

The final results are shown in Fig. 2, together with other recent measurements and the traditional Galster parameterization [10]. Our measurements are limited by

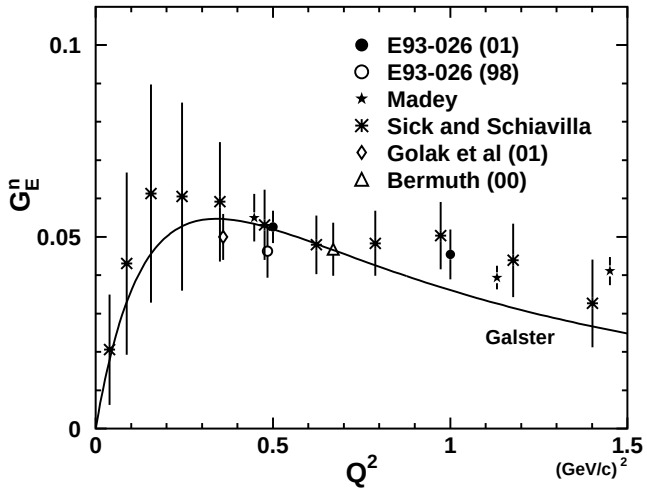

Fig. 2. Recent world data on $G_{\mathrm{E}}^{\mathrm{n}}$. Plotted are the present results (•) and the data from [11] (○), [12] (⋆), [13] (∗), [14] (♢) and [15] (△). The Galster parameterization [10] is shown for reference.

statistics; the smaller systematic errors (5% for $Q^2 = 0.5$ and 8% for 1.0 $(\mathrm{GeV}/c)^2$) are dominated by uncertainties in the beam and target polarizations and the dilution factor. The inherent limitations of the data–MC comparison in $A_{\mathrm{ed}}^{\mathrm{V}}$ are responsible for less than half of our systematic error.

Our new data provide an accurate measurement of $G_{\mathrm{E}}^{\mathrm{n}}$ at the edge of the currently available kinematic range. Together with the other recent measurements, it represents a significant improvement in our knowledge of $G_{\mathrm{E}}^{\mathrm{n}}$ and provides confirmation of the respective methods.

References

[1] T. W. Donnelly and A. S. Raskin, Ann. Phys. (N.Y.) **169** (1986) 247; A. S. Raskin and T. W. Donnelly, Ann. Phys. (N.Y.) **191** (1989) 78.

[2] C. Sinclair, TJNAF Report No. TJNAF-TN-97-021.

[3] M. Hauger et al., Nucl. Inst. Meth. A **462** (2001) 382.

[4] D. Crabb and D. Day, Nucl. Inst. Meth. A **356** (1995) 9; T. D. Averett et al., Nucl. Inst. Meth. A **427** (1999) 440.

[5] D. G. Crabb and W. Meyer, Ann. Rev. Nucl. Part. Sci. **47** (1997) 67.

[6] G. Court, Nucl. Inst. Meth. A **324** (1993) 443.

[7] P. Ulmer, MCEEP: *Monte Carlo for Electro-Nuclear Coincidence Experiments*, Version 3.5.

[8] J. Arrington, SIMC.

[9] H. Arenhövel, W. Leidemann and E. L. Tomusiak, Z. Phys. A **331** (1988) 123; **334** (1989) 363(E); Phys. Rev. C **46** (1992) 455; H. Arenhövel, private communication.

[10] S. Galster et al., Nucl. Phys. B **32** (1971) 221.

[11] H. Zhu et al., Phys. Rev. Lett. **87** (2001) 081801.

[12] R. Madey et al., Phys. Rev. Lett. **91** (2003) 122002.

[13] R. Schiavilla and I. Sick, Phys. Rev. C **64** (2002) 041002(R).

[14] J. Golak et al., Phys. Rev. C **63** (2001) 034006.

[15] J. Bermuth et al., Phys. Lett. B **564** (2003) 199; D. Rohe et al., Phys. Rev. Lett. **83** (1999) 4257.

MJERENJE ELEKTRIČNOG FAKTORA OBLIKA NEUTRONA $G_{\mathrm{E}}^{\mathrm{n}}$ DVOJNO-POLARIZIRANIM KVAZIELESTIČNIM RASPRŠENJEM U JLABU

Odredili smo električni faktor oblika neutrona $G_{\mathrm{E}}^{\mathrm{n}}$ reakcijom $\vec{\mathrm{d}}(\vec{\mathrm{e}}, \mathrm{e}'\mathrm{n})\mathrm{p}$ primjenom uzdužno polariziranog elektronskog snopa i smrznute polarizirane mete $^{15}\mathrm{ND}_3$ u JLabu. Izbačene neutrone opažali smo u hodoskopu od plastičnih scintilatora, sudesno s kvazi-elastično raspršenim elektronima koji su mjereni u spektrometru za velike impulse u Hali C. Da bismo odredili $G_{\mathrm{E}}^{\mathrm{n}}$, usporedili smo mjerenu asimetriju snop-meta s teorijskim računima zasnovamin na više modela $G_{\mathrm{E}}^{\mathrm{n}}$. Izvješćujemo o ishodima od jeseni 2001. na $Q^2 = 0.5$ i 1.0 $(\mathrm{GeV}/c)^2$.